PAPER

Check for updates

A novel metal-free two-dimensional material for photocatalytic water splitting – phosphorus nitride (γ-PN)†

Xiaohong Tan,[a] Yujin Ji, [iD] *[b] Huilong Dong, [iD] [b] Meiyi Liu,[c] Tingjun Hou [iD] [b] and Youyong Li [iD] *[b]

Visible-light-driven water-splitting technology has attracted wide attention because of its sustainable and renewable production of hydrogen. The key to photocatalysis field is to search materials with suitable oxidizing and reducing potential. Herein we investigated the novel 2D γ-phosphorus nitride (γ-PN) monolayer as a candidate photocatalyst for reducing water into hydrogen and oxygen from the first-principles and molecular dynamics calculations. Our results show that the 2D γ-PN monolayer is an indirect semiconductor whose conduction and valence band edges matches well with the chemical potential of H^+/H_2 and O_2/H_2O. Strain effect is considered to tune the electronic properties of γ-PN. The calculation results reveal that tensile strain decreases the band gap and upshifts the work function of the γ-PN monolayer. The γ-PN monolayer at the 10% tensile strain shows the optimal performance in catalysing the water-splitting due to the low band gap and the better absorption spectrum at the UV-visible light range. Furthermore, the molecular dynamics shows that the γ-PN in the aqueous solution always keep stable after 100 ps simulation. Both the density functional theory (DFT) and molecular dynamics (MD) simulation reflect that the γ-PN monolayer is reliable and promising as a water-splitting photocatalyst.

Introduction

The consumer demand for renewable and clean energy is in growth steadily nowadays due to the shortage of exhaustible fossil fuels and the accompanying environmental problems. Seeking alternative environment-friendly energy sources is an effective approach to meet this urgent demand. Hydrogen, as a high-density green energy produced from water splitting with the assistance of sunlight, is considered to balance the energy requirement and environmental protection hopefully in the long term.[1–3] The key to this method is to search high-performance photocatalysts whose band positions should fit the water reduction and oxidation potentials strictly in order to provide a driving force for reducing water.

In the last few decades, a variety of novel nanomaterials are designed as homogeneous and heterogeneous catalysts in the field of catalysis by making use of their high specific surface area and rich active sites. Advanced density functional theory (DFT) calculations have been widely applied to guide the experimenters to understand the fundamental nature of the physical and chemical phenomenon, and to design materials with different structures and optimize the catalytic performance.[4,5] Screening and designing materials with suitable band position through the first-principles calculations play a vital role in current water-splitting studies. The traditional benchmark water-splitting catalyst is the bulk TiO_2 inspired by the pioneering work of Fujishima and Honda.[6,7] However, relatively wide band gap (3 eV in the rutile phase) restricts TiO_2 to making full use of solar energy, resulting in the final less than 1% photoenergy conversion efficiency, which hinders its massive commercial application. Tuning band structure of TiO_2 with externally doped elements is an effective approach to enhance the photocatalysis activity. Both theoretical calculation and experimental results show that doping with 3d transition metal ions (Cr^{3+}, Co^{3+}, Ni^{2+}, Mn^{3+})[8] or non-metal element (B, C, N)[9] will induce doping energy level and change the properties of light absorption obviously.

In recent years, metal-free water-splitting catalysts, such as graphitic carbon nitride (g-C_3N_4), and graphene(G), have spring up due to their distinctive advantages in easy synthesis and no poison. Typically, the g-C_3N_4 investigated by Wang and co-workers are chemically and thermally stable semiconducting materials with direct bandgaps around 2.1 eV, exhibiting steady

[a]College of Mechanical and Electrical Engineering, Hangzhou Polytechnic, Hangzhou 311402, China

[b]Institute of Functional Nano & Soft Materials (FUNSOM), Jiangsu Key Laboratory for Carbon-Based Functional Materials & Devices, Soochow University, Suzhou, 215123, China. E-mail: yujin_ji@163.com; yyli@suda.edu.cn

[c]Suzhou Foreign Language School, Suzhou, 215011, China

† Electronic supplementary information (ESI) available. See DOI: 10.1039/c7ra10305k

2–4% H_2 production efficiency with a small amount Pt content.[10] Meanwhile, compared with the previous TiO_2, these 2D polymeric carbon nitride materials can absorb more visible light due to the narrower bandgap. Furthermore, the doping and defects of g-C_3N_4 and the coupling with other 2D materials can synergistically promote the proton adsorption and reduction kinetic, which shows better photocatalytic performance than that of traditional metallic catalysts.[11–14] Recently, different 2D porous phosphorus polymorphs and transition metal dichalcogenides are also expected as elemental water-splitting photocatalysts with tunable band gaps.[15–17]

To date, the earliest synthesized phosphorus nitride crystal is the α-P_3N_5 and β-α-P_3N_5 made up of the sharing PN_4 tetrahedra, reported by the Wolfgang Schnick et al.[18] A variety of phosphorus nitride compound have been predicted theoretically, such as the PN_2 and PN_3 as superconductor under high pressure.[19] Very recently, we designed novel 2D phosphorus nitride with α, β and γ phases and confirmed that those 2D phosphorus nitride materials are stable and are possible to synthesize at the surface of silver (110), (001) and (111).[20] The 2D PN materials with a 1 : 1 mole fraction of P and N with different electronic and magnetic properties have potentials in the application of nano-electronics.

In this work, we theoretically investigated 2D γ-phosphorus nitride (γ-PN) material as a novel metal-free water-splitting catalyst. This γ-PN nanomaterial is an indirect semiconductor with a bandgap of 2.85 eV based on the HSE06 functional. The conduction band margin (CBM) and valence band margin (VBM) of γ-PN locate energetically around the potential of hydrogen evolution reaction (HER) and oxygen evolution reaction (OER), indicating their great potentials in metal-free photocatalytic water splitting. Strain effect is considered to enhance the photocatalysis performance. In addition, this γ-PN keep stable after 100 ps molecular dynamics simulation at 300 K in the aqueous environment.

Computational details

All the DFT calculations are performed by the CASTEP module[21] in the Materials Studio (version 8.0). The generalized gradient approximation (GGA) realized by Perdew–Burke–Ernzerhof (PBE)[22] functional with norm-conserving pseudopotentials[23] was used to optimize all the structures. Grimme correction method[24] was used to describe the van der Waals interaction. The valence electron for N and P was $2s^2p^3$ and $3s^23p^3$. The cut-off energy was set to 500 eV and the convergence criteria are 5.0×10^{-6} eV per atom for energy and 0.01 eV Å^{-1} for force, which are enough to ensure reasonable simulation results. Over 20 Å vacuum slab is used to avoid the interaction between neighboring layers. The 13 × 13 × 1 K-points were used in the geometry optimization and self-consistent calculations for the density of states (DOS) and band structure. Considering traditional GGA-PBE may underestimate the band gap of 2D materials, advanced hybrid functional Heyd–Scuseria–Ernzerhof (HSE06)[25] was used to correct the band gap with a 7 × 7 × 1 K-points.

The absorption spectrum is calculated by the frequency dependent dielectric matrix, where the real part $\varepsilon_1(\omega)$ is obtained by the Kramers–Kronig transformation and the imaginary part $\varepsilon_2(\omega)$ is determined by a summation over empty states using the following equation:[26,27]

$$\varepsilon_2 = \frac{2\pi e^2}{\Omega \varepsilon_0} \sum_{k,v,c} \left| \langle \varphi_k^c | \boldsymbol{u} \cdot \boldsymbol{r} | \varphi_k^v \rangle \right|^2 \delta \left(E_k^c - E_k^v - E \right)$$

where the indices c and v refer to conduction and valence band states, respectively. φ_k^c is the cell periodic part of the orbitals at the k point in the Brillouin zone and the $\boldsymbol{u}$ is the vector defining the polarization of the incident electric field. The absorption coefficient $A(\omega)$ is defined as following:

$$A(\omega) = \frac{\sqrt{2}\omega}{c} \left[\left(\varepsilon_1^2 + \varepsilon_2^2 \right)^{1/2} - \varepsilon_1 \right]^{1/2}$$

Molecular dynamics of 4 × 4 γ-PN supercells surrounded with water molecules at 300 K under the canonical ensemble (NVE) was run to estimate the thermodynamic stability and the total simulation time is set as 100 ps. The COMPASS[28] force field is chosen, which is compatible with our first-principles calculations. The electrostatic interaction and van der Waals interaction used the atom based method.

Results and discussion

Based on our previous work,[20] there are three types of stable PN monolayers, individually α-, β-, and γ-PN. All of them show highly structural and dynamic stability. The formation enthalpy of γ-PN is calculated to be negative (−0.08 eV), suggesting its existence in reality is possible. As shown in Fig. 1, the γ-PN forms a graphene-like hexagonal lattice where the bond length between N and P is uniformly 1.79 Å. The valence electrons in the outer layer of N ($2p^3$) and P ($3p^3$) atom result in covalent bonding between N and P according to the bond order of 0.84. The larger electronegativity of N atom than P atom indicates the transfer of electrons from P atoms to N atoms during the formation of γ-PN. Similar to black phosphorus and varieties of phosphorus allotropes, the P atoms are sp^2 hybridized with three neighboring N atoms by the covalent bond, which stabilized the whole framework in principles. Then advanced hybrid density functional HSE06 is adopted to calculate the band structure and partial density of states because traditional GGA and LDA functionals will underestimate about ∼1.0 eV in band gap for 2D materials. The band gap of the γ-PN monolayer is 2.85 eV from the advanced hybrid density functional HSE06 compared with 1.72 eV from GGA-PBE calculation. The PDOS shows a hybrid character of p orbitals from N and P atoms in the γ-PN configuration, which contributes to 3-fold coordination typically. While for α-PN and β-PN monolayer, they are also indirect semiconductors with a corresponding band gap of 2.61 eV and 2.29 eV shown in Fig. S1 of ESI.† Fig. S1c† shows that the valance band maximum of α-PN and β-PN is −5.29 eV and −5.09 eV respectively, both of which are higher than the oxidation potential of water ($E_{H_2O/O_2} = -5.67$ eV) and have little potential in the water splitting.

As we know, most photoelectric devices made by 2D materials should deposit on different substrates. On the one hand,
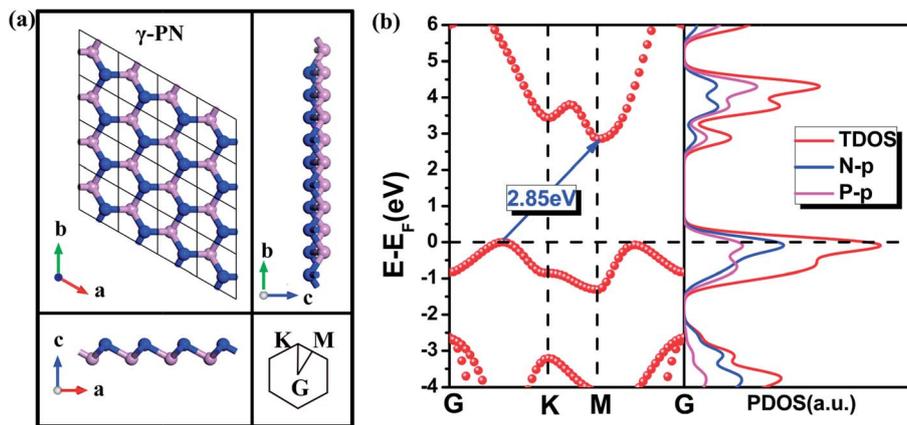
Fig. 1 (a) The top view and side view of 2D γ-PN monolayer, as well as the corresponding path in the Brillouin zones and (b) the band structure and partial density of states of γ-PN based on the HSE06 functional (pink and blue balls represent the phosphorus and nitrogen atoms respectively).

the substrates are propitious to protect and stabilize the 2D materials. On the other hand, the lattice mismatch between substrates and 2D materials is also an effective way to tune the photoelectric properties of 2D materials,[29,30] which arises the importance of strain effect. Considering the successful synthesis of silicene on Ag substrates,[31] it is predicted that three monolayer PN nanosheets deposited on the Ag substrate by CVD with cyclic phosphazenes in our previous work with a roughly 2%–13% lattice mismatch where the Ag substrate can stabilize the growth of monolayer PN.[20] Here, the strain effect is considered by changing the lattice parameter in proportion, and the corresponding electronic properties are tailored simultaneously. The tensile/compressive strain is defined as $\varepsilon = (a - a_0)/a_0$, where a and a_0 are the lattice constants of the relaxed and strained structure, respectively. Firstly, the ideal strength of 2D PN allotropes are determined by the stress–strain relationship and the maximum stress corresponds to the instability point.[32,33] As shown in Fig. 2, the ideal strength of γ-PN along uniaxial direction is 12% strain, corresponding to a maximum stress of 4.33 GPa.

Secondly, the strain effect on electronic properties of 2D γ-PN monolayer is taken into consideration. Introducing strain into 2D materials will not only change the structure, but also cause the electronic redistribution and further alter the band gap of 2D semiconductor materials. Here strains ranging from

−10% (compressive) to +10% (tensile) are considered in our calculations because that the γ-PN shows a maximum strain higher than 10%, so that strains in this range could assure the stability of γ-PN. Fig. 3 shows the varying tendency of the bandgap of γ-PN monolayer based on the HSE06 functional. It should be noted that the chosen functional (HSE06 or PBE) do not influence the common tendency of band gap against the applied strain. A band gap range of 1.2–3.2 eV is tuned by strain with the type of band structure keeps indirect. At the strain range from −5% to 10%, the band gap will linearly decrease. Band gap at the −5% compressive strain and +10% tensile strain corresponds to the maximum (3.1 eV) and the minimum (2.27 eV). Furthermore, the energy position of VBM and CBM are considered. The VBM is viewed as the work function of 2D materials, calculated from the difference between the vacuum level (set as 0) and Fermi level of 2D materials determined by the GGA-PBE functional. The band gap obtained by HSE06 functional is then used to locate the position of CBM.[34] According to Fig. 3b, the VBM and CBM level of the original γ-PN monolayer are −6.82 eV and −3.98 eV respectively. The work function of γ-PN shows different varying tendency from the band gap and will have a little upshift under the tensile strain. Both VBM level and band gap lead to the decrease of CBM of the γ-PN. It should be noted that the standard reduction potential of H^+/H_2 and oxidation potential of O_2/H_2O is −4.44 eV and −5.67 eV relative to the vacuum level, which is a determining factor of water-splitting materials driven by visible light.[35] With the increased tensile strain, band gap of the γ-PN monolayer linearly decreases and the work function of γ-PN monolayer increase gradually, which is useful to enhance the performance of the γ-PN.

Fig. 4a plots the band edge alignment of the γ-PN monolayer with respect to the Standard Hydrogen Electrode (SHE). The redox potential of H^+/H_2 changes to 0 eV and the redox potential of O_2/H_2O is set to 1.23 eV relative to the SHE. At ambient condition without strain, the VBM and CBM of γ-PN locate around the redox potential of H^+/H_2 and O_2/H_2O, which can provide a driven force for the oxidation and reduction reaction.
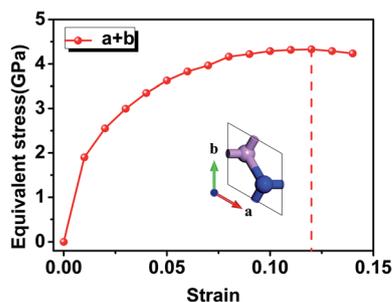

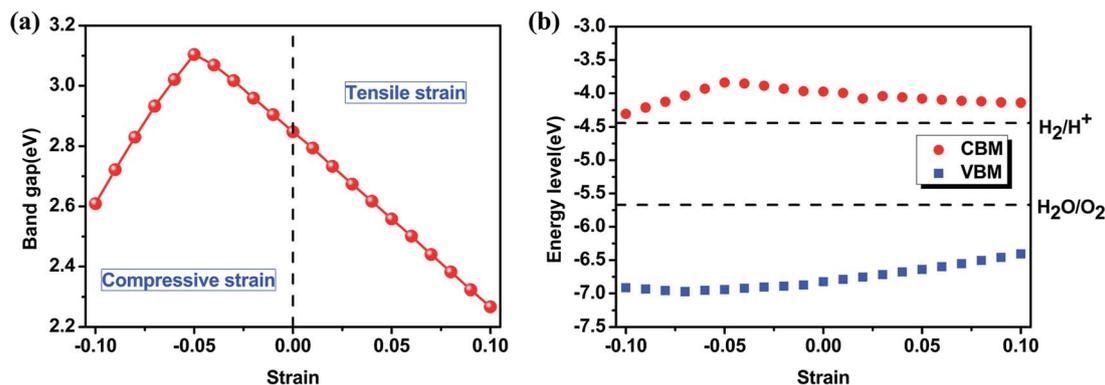**Fig. 2** Stress–strain curves of 2D γ-PN monolayer.

Fig. 3 (a) The band gap of γ-PN monolayer as a function of the uniaxial strain and (b) the located position of VBM and CBM.
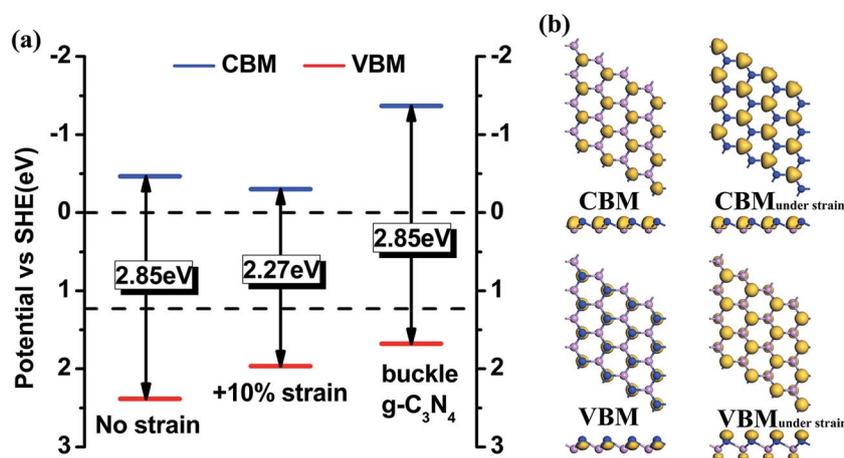

Fig. 4 (a) Energy alignment of the γ-PN monolayer with no strain and under 10% tensile strain when pH = 0 and (b) the wave function distribution of VBM and CBM of γ-PN monolayer with no strain and 10% tensile strain.

With the introduced tensile strain, the decrease of the band gap and the upshift of VBM will decrease the difference between the VBM of γ-PN and the redox potential of H_2O, which helps to keep the balance of water-splitting reaction. Especially, the γ-PN with +10% tensile strain shows a narrower band gap (2.27 eV) and suitable band alignment, which indicates its better performance in photocatalysis of water splitting. The wave function distribution of VBM and CBM of γ-PN are given in Fig. 4b. It is found that the CBM and VBM at the situation of no strain are mainly contributed by the nitrogen atoms. The CBM and VBM distribution of γ-PN have a little overlapping, which is unfavourable for carriers to diffuse. However, the CBM distribution at the +10% tensile strain localizes to the phosphorus atoms, which helps to decrease the orbital overlapping efficiently. The less overlapping between CBM and VBM as well as narrower band gap caused by strain is beneficial to the separation and diffusion of charge carriers and could make full use of them, thus enhancing the catalysing activity. Our calculations indicate that strain engineering of the γ-PN monolayer is a useful way to improve the performance of photocatalysis.

In addition, we compared the optical properties of γ-PN and previously studied graphitic carbon nitride (g-C_3N_4) monolayer

based on the HSE06 functional. Fig. 5 displays the absorption spectra as the function of photon energy in the vertical direction of the plane. It is found that the main absorption peaks of the γ-PN and g-C_3N_4 monolayer widely locate at the ultraviolet area because of their relatively large band gap. Although the band gap

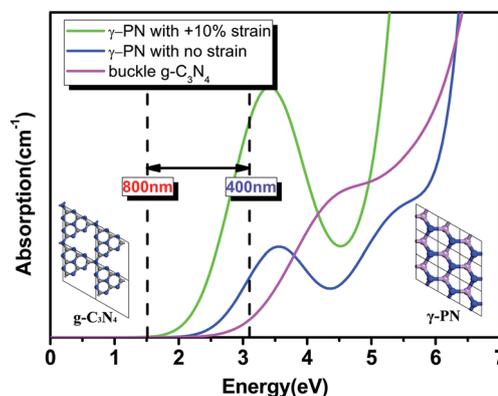**Fig. 5** The absorption coefficient of γ-PN and buckle g-C_3N_4 along the vertical direction of 2D materials.
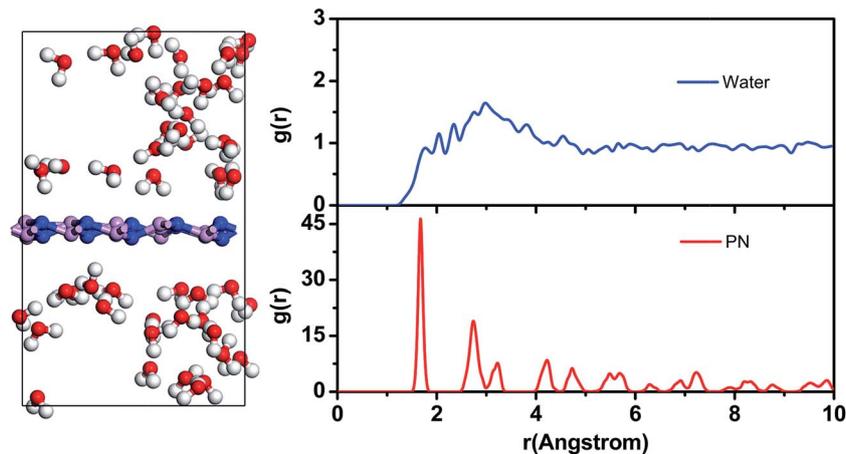
Fig. 6 Snapshot of phosphorus nitride in liquid water and the radius distribution function $g(r)$ after 100 ps molecular dynamics at 300 K (the pink, blue, red and white balls present the P, N, O, and H atoms, respectively).

of the γ-PN and g-C$_3$N$_4$ monolayer is about 2.85 eV, the γ-PN shows wider and higher absorption intensity than that of g-C$_3$N$_4$ at the range between 1.55 eV and 3.1 eV, corresponding to the visible light area (about 400 nm–800 nm in wavelength). Moreover, the absorption peaks of γ-PN at the +10% tensile strain shows more overlapping with visible light area and stronger absorption for visible light compare with g-C$_3$N$_4$ monolayer, equipping the better absorption coefficients with the low band gap of 2.27 eV. Specifically, for γ-PN at the +10% tensile strain there is an enhanced peak located at about 3.5 eV, showing its superior absorption on near-ultraviolet light. The above results reveal that the tensile strain will further enhance the photocatalysis performance of water splitting for γ-PN, which provides a versatile way to tune its optoelectronic properties.

Furthermore, we simulated the interfacial water decomposition on the γ-PN monolayer in order to unfold the microscopic mechanism shown in Fig. S2 of ESI.† The adsorption of water molecule is weak interaction −0.27 eV while the following water decomposition is an endothermic reaction with a reaction energy of 1.24 eV (from −0.27 eV to 0.97 eV), which is comparable to the water splitting reaction on the 2D Zr$_2$CO$_3$ and TiO$_2$ surface. Moreover, the ultra-high specific surface area of PN monolayer with a board visible light absorption is available to enhance the performance of photocatalytic reactions compared to the bulk TiO$_2$ and 2D g-C$_3$N$_4$.

Last but not least, we run 100 ps molecular dynamics to investigate the structural stability of γ-PN monolayer configurations under the surrounding of water. The constructed periodical box ensures the 1 g cm^{-2} density in the whole system. It is clearly found that the γ-PN monolayer is still stable in the environment of H$_2$O after 100 ps molecular dynamics simulation at 300 K, as shown in Fig. 6. Furthermore, the radius distribution function $g(r)$ of P–N and H$_2$O are investigated to characterize how the densities of water molecules and N–P varies as a function of space distance and the discrete peaks in Fig. 6 show well crystalline γ-PN and the distance between water molecules are about 1 Å, which is the intrinsic distance of liquid water in the solution and agrees well with the previous XRD measurements.[36]

Conclusions

In this work, novel γ-PN monolayer is investigated as a visible-light-driven water-splitting photocatalyst based on the first-principles calculations. We verify that the γ-PN monolayer is an indirect semiconductor with a bandgap of 2.85 eV. The VBM and CBM of γ-PN monolayer are −6.82 eV and −3.98 eV respectively and are located around the reduction and oxidation potentials of H$_2$O energetically, enabling the γ-PN monolayers as effective and promising metal-free visible-light-driven water-splitting photocatalysts. Meanwhile, the band gap and energy levels of γ-PN can be effectively tuned by the external applied strain effect. The γ-PN monolayer at the 10% tensile strain shows the optimal water-splitting performance due to the low band gap and the superior absorption on UV-visible light. In addition, the stability of γ-PN monolayer in aqueous solution is considered by the molecular dynamics and confirms the reliability of γ-PN monolayer in splitting water. The novel γ-PN nanomaterial has shown good potential in catalysing visible-light-driven water-splitting and is promising as a metal-free photocatalyst if be synthesized.

Conflicts of interest

There are no conflicts to declare.

Acknowledgements

References

1 Y. Xu, M. Kraft and R. Xu, Metal-free carbonaceous electrocatalysts and photocatalysts for water splitting, *Chem. Soc. Rev.*, 2016, **45**, 3039–3052.

2 X. X. Zou and Y. Zhang, Noble metal-free hydrogen evolution catalysts for water splitting, *Chem. Soc. Rev.*, 2015, **44**, 5148–5180.

3 H. Li, C. Tsai, A. L. Koh, L. L. Cai, A. W. Contryman, A. H. Fragapane, J. H. Zhao, H. S. Han, H. C. Manoharan, F. Abild-Pedersen, J. K. Norskov and X. L. Zheng, Activating and optimizing MoS2 basal planes for hydrogen evolution through the formation of strained sulphur vacancies, *Nat. Mater.*, 2016, **15**, 48–53.

4 S. Zhang, Z. Yan, Y. Li, Z. Chen and H. Zeng, Atomically thin arsenene and antimonene: semimetal-semiconductor and indirect-direct band-gap transitions, *Angew. Chem., Int. Ed.*, 2015, **54**, 3112–3115.

5 Y. Qu and X. Duan, Progress, challenge and perspective of heterogeneous photocatalysts, *Chem. Soc. Rev.*, 2013, **42**, 2568–2580.

6 A. Fujishima, X. T. Zhang and D. A. Tryk, TiO2 photocatalysis and related surface phenomena, *Surf. Sci. Rep.*, 2008, **63**, 515–582.

7 A. F. a. K. Honda, Electrochemical photolysis of water at a semiconductor electrode, *Nature*, 1972, **238**, 37–38.

8 W. Choi, A. Termin and M. R. Hoffmann, The Role of metal ion dopants in quantum-sized TiO_2: Correlation between photoreactivity and charge carrier recombination dynamics, *J. Phys. Chem.*, 1994, **98**, 13669–13679.

9 C. Di Valentin and G. Pacchioni, Trends in non-metal doping of anatase TiO_2: B, C, N and F, *Catal. Today*, 2013, **206**, 12–18.

10 X. Wang, K. Maeda, A. Thomas, K. Takanabe, G. Xin, J. M. Carlsson, K. Domen and M. Antonietti, A metal-free polymeric photocatalyst for hydrogen production from water under visible light, *Nat. Mater.*, 2009, **8**, 76–80.

11 Y. Zheng, Y. Jiao, Y. Zhu, L. H. Li, Y. Han, Y. Chen, A. Du, M. Jaroniec and S. Z. Qiao, Hydrogen evolution by a metal-free electrocatalyst, *Nat. Commun.*, 2014, **5**, 3783.

12 W. Cui, J. Li, W. Cen, Y. Sun, S. C. Lee and F. Dong, Steering the interlayer energy barrier and charge flow via biorented transportation channels in g-C 3 N 4 : Enhanced photocatalysis and reaction mechanism, *J. Catal.*, 2017, **352**, 351–360.

13 T. Xiong, W. Cen, Y. Zhang and F. Dong, Bridging the g-C3N4 Interlayers for Enhanced Photocatalysis, *ACS Catal.*, 2016, **6**, 2462–2472.

14 P. Li, W. Zhang, Y. Zhang, Y. Sun and F. Dong, (NH4)2SO4-assisted polycondensation of dicyandiamide for porous g-C3N4with enhanced photocatalytic NO removal, *RSC Adv.*, 2016, **6**, 96334–96338.

15 Z. Zhuo, X. Wu and J. Yang, Two-Dimensional Phosphorus Porous Polymorphs with Tunable Band Gaps, *J. Am. Chem. Soc.*, 2016, 7091–7098.

16 H. L. Zhuang and R. G. Hennig, Computational Search for Single-Layer Transition-Metal Dichalcogenide Photocatalysts, *J. Phys. Chem. C*, 2013, **117**, 20440–20445.

17 Y. Jiao, L. Zhou, F. Ma, G. Gao, L. Kou, J. Bell, S. Sanvito and A. Du, Predicting Single-Layer Technetium Dichalcogenides (TcX2, X = S, Se) with Promising Applications in Photovoltaics and Photocatalysis, *ACS Appl. Mater. Interfaces*, 2016, **8**, 5385–5392.

18 W. Schnick and J. L. c. Frank Krumeich., Phosphorus Nitride P3N5: Synthesis, Spectroscopic, and Electron Microscopic Investigations, *Chem. Mater.*, 1996, **8**, 281–286.

19 Z. Raza, I. Errea, A. R. Oganov and A. M. Saitta, Novel superconducting skutterudite-type phosphorus nitride at high pressure from first-principles calculations, *Sci. Rep.*, 2014, **4**, 5889.

20 S. Ma, C. He, L. Z. Sun, H. Lin, Y. Li and K. W. Zhang, Stability of two-dimensional PN monolayer sheets and their electronic properties, *Phys. Chem. Chem. Phys.*, 2015, **17**, 32009–32015.

21 M. D. Segall, P. J. D. Lindan, M. J. Probert, C. J. Pickard, P. J. Hasnip, S. J. Clark and M. C. Payne, First-principles simulation: ideas, illustrations and the CASTEP code, *J. Phys.: Condens. Matter*, 2002, **14**, 2717–2744.

22 J. P. Perdew, K. Burke and M. Ernzerhof, Generalized gradient approximation made simple, *Phys. Rev. Lett.*, 1996, **77**, 3865–3868.

23 D. R. Hamann, M. Schluter and C. Chiang, Norm-Conserving Pseudopotentials, *Phys. Rev. Lett.*, 1979, **43**, 1494–1497.

24 S. Grimme, Semiempirical GGA-type density functional constructed with a long-range dispersion correction, *J. Comput. Chem.*, 2006, **27**, 1787–1799.

25 J. Heyd, G. E. Scuseria and M. Ernzerhof, Hybrid functionals based on a screened Coulomb potential, *J. Chem. Phys.*, 2003, **118**, 8207–8215.

26 P. Rani, G. S. Dubey and V. K. Jindal, DFT study of optical properties of pure and doped graphene, *Phys. E*, 2014, **62**, 28–35.

27 M. Gajdos, K. Hummer, G. Kresse, J. Furthmuller and F. Bechstedt, Linear optical properties in the projector-augmented wave methodology, *Phys. Rev. B: Condens. Matter Mater. Phys.*, 2006, **73**, 9.

28 H. Sun, COMPASS: An ab initio force-field optimized for condensed-phase applications - Overview with details on alkane and benzene compounds, *J. Phys. Chem. B*, 1998, **102**, 7338–7364.

29 C. R. Dean, A. F. Young, I. Meric, C. Lee, L. Wang, S. Sorgenfrei, K. Watanabe, T. Taniguchi, P. Kim, K. L. Shepard and J. Hone, Boron nitride substrates for high-quality graphene electronics, *Nat. Nanotechnol.*, 2010, **5**, 722–726.

30 G. Giovannetti, P. A. Khomyakov, G. Brocks, P. J. Kelly and J. van den Brink, Substrate-induced band gap in graphene on hexagonal boron nitride: Ab initio density functional calculations, *Phys. Rev. B: Condens. Matter Mater. Phys.*, 2007, **76**, 4.

31 J. Gao and J. Zhao, Initial geometries, interaction mechanism and high stability of silicene on Ag(111) surface, *Sci. Rep.*, 2012, **2**, 861.

32 D. Roundy and M. L. Cohen, Ideal strength of diamond, Si, and Ge, *Phys. Rev. B: Condens. Matter Mater. Phys.*, 2001, **64**, 3.

33 S. Guan, Y. Cheng, C. Liu, J. Han, Y. Lu, S. A. Yang and Y. Yao, Effects of strain on electronic and optic properties of holey two-dimensional C2N crystals, *Appl. Phys. Lett.*, 2015, **107**, 231904.

34 X. Jiang, J. Nisar, B. Pathak, J. Zhao and R. Ahuja, Graphene oxide as a chemically tunable 2-D material for visible-light photocatalyst applications, *J. Catal.*, 2013, **299**, 204–209.

35 X. Li, Z. Li and J. Yang, Proposed photosynthesis method for producing hydrogen from dissociated water molecules using incident near-infrared light, *Phys. Rev. Lett.*, 2014, **112**, 018301.

36 A. H. Harten, M. D. Danford and H. A. Levy, X-Ray Diffraction Study of Liquid Water in the Temperature Range 4-200°C, *Discuss. Faraday Soc.*, 1967, **43**, 97–107.